ESTA JOURNAL
Energy Storage Technology and Applications
Article
jurnal.uns.ac.id/esta

Isothermal Decomposition Kinetics of NMC 622 and NCA Oxalate Precursors During Calcination for Lithium-Ion Cathode Preparation

K. N. R. Stulasti[1], A. D. Rahmawati[1], L. N. Aini[1], A. Fitriani[1], N. Zamruda[1], H. S. E. A. Gustiana[1], and C. S. Yudha[1*]

1. Chemical Engineering Department, Vocational School, Universitas Sebelas Maret, Jl. Kol. Sutarto 150K Jebres, Surakarta 57126, Indonesia

* Corresponding author: corneliussyudha@staff.uns.ac.id

doi: https://doi.org/10.20961/esta.v4i2.117683
Received: 20-04-2026; Revised: 27-04-2026; Accepted: 31-05-2026; Published: 17-06-2026

ABSTRACT: Oxalate precursors for NMC 622 ($Ni_{0.6}Mn_{0.2}Co_{0.2}$) and NCA ($Ni_{0.8}Co_{0.15}Al_{0.05}$) cathode materials were synthesized by co-precipitation at 60 °C and pH 2.0, then subjected to isothermal calcination at 350, 400, and 450 °C. Mass-loss data collected at 10-minute intervals were analyzed using the integral kinetic method to determine reaction order, rate constants, and Arrhenius parameters. NMC 622 decomposition followed first-order kinetics with rate constants of 0.0043–0.0104 min^{-1} and an activation energy of 19.66 kJ mol^{-1}. NCA decomposition obeyed zero-order kinetics with rate constants of 0.0674–0.2329 g min^{-1} and a higher activation energy of 50.63 kJ mol^{-1}. The contrasting kinetic behaviours indicate distinct rate-controlling mechanisms for the two precursor chemistries. To the authors' knowledge, this study provides the first systematic isothermal kinetic characterisation of mixed-metal NMC 622 and NCA oxalate precursors, yielding quantitative parameters directly applicable to the design and optimisation of calcination schedules in battery-grade cathode manufacturing.

Keywords: calcination, decomposition kinetics, NMC 622, NCA, activation energy, Arrhenius, oxalate precursor, battery cathode, co-precipitation.

1. INTRODUCTION

The global transition towards electrified transportation and grid-scale energy storage has intensified demand for high-energy-density lithium-ion batteries (LIBs). Among cathode chemistries, layered oxide materials based on nickel–manganese–cobalt (NMC) and nickel–cobalt–aluminium (NCA) are commercially dominant owing to their favourable combination of specific capacity, structural stability, and thermal performance [1,2]. The electrochemical performance of these cathode materials is critically dependent on the physicochemical quality of their precursors and the subsequent thermal processing conditions [3].

Cathode precursors are typically produced as hydroxide or carbonate co-precipitates; however, oxalate co-precipitation offers an attractive alternative route due to its precise stoichiometric control, lower processing temperatures, and the generation of gas-

phase decomposition products (CO, CO_2, H_2O) that leave minimal impurity residues in the final oxide [4,5]. The metal oxalate precursor decomposes during calcination to yield the mixed metal oxide, which is subsequently lithiated at high temperature to form the layered cathode phase.

Calcination is a critical unit operation that determines the microstructure, phase purity, and surface chemistry of the resulting oxide powder [6]. Inadequate calcination produces incomplete decomposition and residual oxalate phases, while excessive temperature leads to particle sintering, cation disordering, and surface rock-salt formation — all of which degrade electrochemical performance [7,8]. A quantitative understanding of the decomposition kinetics is therefore essential for rational process design and scale-up.

Kinetic studies of solid-state decomposition are most commonly conducted under isothermal or non-isothermal (ramped) conditions. The isothermal approach, in which the sample is rapidly equilibrated at a fixed temperature and mass loss is monitored over time, yields rate constants and activation energies through straightforward application of the Arrhenius equation and is particularly suited to batch-furnace laboratory conditions [9]. Several studies have investigated the decomposition kinetics of simple binary oxalates (e.g., NiC_2O_4, CoC_2O_4) [10,11]; however, data on ternary and quaternary mixed-metal oxalate precursors representative of commercial NMC and NCA compositions remain limited.

In this work, NMC 622 ($Ni_{0.6}Mn_{0.2}Co_{0.2}(C_2O_4)\cdot 2H_2O$) and NCA ($Ni_{0.8}Co_{0.15}Al_{0.05}(C_2O_4)\cdot 2H_2O$) precursors were synthesised by oxalate co-precipitation and subjected to isothermal calcination across a temperature window of 350–450 °C. Rate constants were determined by fitting the integral kinetic model, and the temperature dependence was quantified via the Arrhenius equation to extract activation energies and pre-exponential factors. The results are discussed in the context of decomposition mechanism and their implications for calcination process design.

2. MATERIALS AND METHODS

2.1 Material

All chemicals were used without additional purification. Table 1 provides a complete list of reagents, their commercial suppliers, purity grades, and functions in the synthesis.

Table 1. Reagents used in co-precipitation and calcination experiments

Chemical	Supplier	Purity / Grade	Role in Synthesis
$NiSO_4\cdot 6H_2O$	Zenith	Technical	Ni^{2+} source
$CoSO_4$	Rubamin	Technical	Co^{2+} source
$MnSO_4\cdot H_2O$	—	Technical	Mn^{2+} source (NMC 622 only)
$Al_2(SO_4)_3\cdot 18H_2O$	Bratachem	Technical	Al^{3+} source (NCA only)
$H_2C_2O_4$ (Oxalic acid)	Merck	PA	Precipitating / complexing agent
$NaOH$	Asahi	Technical	pH control (target pH 2.0)
Deionised water	—	18.2 MΩ·cm	Solvent and wash medium

2.2 Methodology

2.2.1 Oxalate Precursor Synthesis

Two precursor compositions were targeted: NMC 622 ($Ni_{0.6}Mn_{0.2}Co_{0.2}$) and NCA ($Ni_{0.8}Co_{0.15}Al_{0.05}$). For NMC 622, aqueous sulfate solutions of $NiSO_4 \cdot 6H_2O$ (Zenith), $CoSO_4$ (Rubamin), and $MnSO_4 \cdot H_2O$ were prepared and combined in a Ni Mn Co molar ratio of 6 : 2 : 2 to give a total transition-metal concentration of 0.5 mol L^{-1}. For NCA, $NiSO_4 \cdot 6H_2O$, $CoSO_4$, and $Al_2(SO_4)_3 \cdot 18H_2O$ (Bratachem) were combined in the molar ratio Ni Co Al = 8 : 1.5 : 0.5.

Oxalic acid (Merck, PA grade) dissolved in deionised water was added to each metal sulphate solution as the precipitating agent at a metal-to-oxalate molar ratio of 1 : 1, in accordance with the stoichiometry of the target oxalate phase. The mixture was stirred continuously at 60 °C. NaOH solution (Asahi) was added dropwise to adjust and maintain the pH at 2.0 ± 0.1, measured with a calibrated pH electrode. This mildly acidic pH was deliberately chosen to ensure selective oxalate precipitation while suppressing competing hydroxide formation, which becomes thermodynamically favoured above pH 5 for Ni^{2+} and Co^{2+} [4]. Al^{3+} begins to precipitate as $Al(OH)_3$ above pH ~ 4 [12], so maintaining pH 2 also prevents premature Al hydroxide formation that would lead to compositional heterogeneity.

The co-precipitation reactions for the constituent metals can be written as:

$$Ni^{2+} + C_2O_4^{2-} + 2H_2O \longrightarrow NiC_2O_4 \cdot 2H_2O\downarrow \quad (1)$$

$$Co^{2+} + C_2O_4^{2-} + 2H_2O \longrightarrow CoC_2O_4 \cdot 2H_2O\downarrow \quad (2)$$

$$Mn^{2+} + C_2O_4^{2-} + 2H_2O \longrightarrow MnC_2O_4 \cdot 2H_2O\downarrow \quad (3)$$

$$2Al^{3+} + 3C_2O_4^{2-} + 6H_2O \longrightarrow Al_2(C_2O_4)_3 \cdot 6H_2O\downarrow \quad (4)$$

Under co-precipitation conditions, the metal ions are simultaneously incorporated into a mixed oxalate solid solution, so that the as-precipitated powder has a single-phase structure with the general formula $M(C_2O_4) \cdot 2H_2O$, where M represents the weighted-average transition metal composition [13]. The precipitate was collected by vacuum filtration, washed three times with deionized water to remove residual sulfate ions, and dried at 80 °C for 12 h in a convective oven.

2.2.2 Isothermal Calcination Experiments

Calcination was conducted in a muffle furnace (resistance-heated) at three target temperatures: 350, 400, and 450 °C. Each experiment began with preheating the empty furnace to the target temperature and allowing it to stabilize for at least 15 minutes. Approximately 10.0 g of dried precursor powder was placed in a pre-tared porcelain crucible. The crucible was inserted into the furnace, and the start time t_0 was recorded. At 10-minute intervals, the crucible was withdrawn, immediately weighed on an analytical balance (±0.01 g), and returned to the furnace. The experiment was terminated when two consecutive weighing differed by less than 0.02 g, indicating that decomposition was practically complete. Both NMC 622 and NCA precursors were studied at each temperature.

The overall thermal decomposition of a generic divalent metal oxalate dihydrate proceeds according to:

$$MC_2O_4 \cdot 2H_2O_{(s)} \longrightarrow MO_{(s)} + CO_{(g)} + CO_{2\,(g)} + 2H_2O_{(g)} \quad (5)$$

where M represents the mixed transition metal. This reaction is endothermic and involves simultaneous dehydration of crystal water and thermal cleavage of the oxalate C–C and C–O bonds. For aluminium, the product is the corresponding oxide Al_2O_3 rather than a divalent oxide:

$$Al_2(C_2O_4)_3{\cdot}6H_2O_{(s)} \longrightarrow Al_2O_{3\,(s)} + 3CO_{(g)} + 3CO_{2\,(g)} + 6H_2O_{(g)} \quad (6)$$

The theoretical final mass fraction (residual oxide relative to initial oxalate) can be estimated from stoichiometry. For $NiC_2O_4{\cdot}2H_2O$ (M_r = 182.7 g mol^{-1}) decomposing to NiO (M_r = 74.7 g mol^{-1}), the theoretical mass retention is 74.7/182.7 = 40.9 %. Comparable values apply to Co and Mn oxalates, so the expected final mass of the NMC 622 oxide product is approximately 41 % of the initial precursor mass, consistent with the experimentally observed stable plateau masses of 3.8–4.2 g (38–42 %).

2.2.3 Kinetic Analysis — Integral Method

The solid-state decomposition was treated as a pseudo-homogeneous batch reaction in which the instantaneous precursor mass W(t) serves as the concentration proxy. Two limiting rate laws were tested:

$$\text{Zero-order } (\alpha = 0): \quad -dW/dt = k_0 \quad \longrightarrow \quad W_0 - W_t = k_0\, t \quad (7)$$

$$\text{First-order } (\alpha = 1): \quad -dW/dt = k_1 W \quad \longrightarrow \quad \ln(W_0/W_t) = k_1\, t \quad (8)$$

where W_0 = 10.0 g is the initial precursor mass and W_t is the mass at time t (min). The rate constant k was extracted as the slope of the respective linearised plot fitted through the origin. Model selection was based on the coefficient of determination R^2: the model with R^2 closer to unity was retained as the superior description of the decomposition behaviour at each temperature.

The temperature dependence of k was described by the Arrhenius equation:

$$k = A{\cdot}\exp(-E_a/RT) \quad (9)$$

which in linearised form gives:

$$\ln k = \ln A - (E_a/R)(1/T) \quad (10)$$

where E_a is the activation energy (J mol^{-1}), A is the pre-exponential frequency factor, R = 8.314 J mol^{-1} K^{-1}, and T is the absolute temperature (K). The slope of the linear regression of ln k vs. 1/T was used to compute E_a = −slope × R, and the intercept gave A = exp(intercept). Statistical quality of the Arrhenius fit was assessed by the coefficient of determination R^2 of the ln k vs. 1/T regression.

3. RESULTS AND DISCUSSION

3.1 Precursor Synthesis

Co-precipitation at pH 2.0 and 60 °C yielded fine, light-green (NMC 622) and turquoise-green (NCA) powders, consistent with the characteristic colours of mixed Ni/Co/Mn and Ni/Co oxalate phases reported in the literature [14]. Both precipitates were highly filterable, indicating adequate particle size and low colloidal character at the chosen pH. The selected conditions represent a compromise: sufficient acidity to suppress hydroxide formation, but enough deprotonation of oxalic acid (pK_{a1} = 1.25, pK_{a2} = 4.27 [15]) to maintain an oxalate dianion activity adequate for precipitation. At pH 2, the predominant oxalate species in solution is $HC_2O_4^-$ rather than $C_2O_4^{2-}$; however, the elevated temperature (60 °C) increases the equilibrium solubility product of the metal oxalates, promoting incorporation of all metal ions into the co-precipitate at comparable rates [16].

The 1 : 1 metal-to-oxalate stoichiometric ratio ensures complete co-precipitation without excess free oxalate remaining in solution, which could otherwise cause post-precipitation during drying. Washing with deionized water removed residual SO_4^{2-} ions that would otherwise act as sintering aids during calcination [3]. The precursor powders were single-phase, as assessed by visual and gravimetric methods, with the NMC

622 and NCA powders yielding stable dried masses close to the theoretical oxalate dihydrate formula weight.

3.2 Isothermal Mass-Loss Profiles

Figure 1 displays the mass of NMC 622 and NCA precursors as a function of calcination time at 350, 400, and 450 °C. In all cases, the decomposition follows a characteristic two-stage profile. An initial rapid mass-loss phase occurs within the first 20–40 minutes, corresponding to overlapping dehydration of crystal water and onset of oxalate thermal cleavage. A second, progressively decelerating phase follows as the remaining oxalate content diminishes and the growing product oxide layer impedes further reaction. Mass stabilization, signaling effective completion of decomposition, was reached within approximately 80–100 minutes at 350 °C, 70–80 minutes at 400 °C, and 30–40 minutes at 450 °C for both precursors.

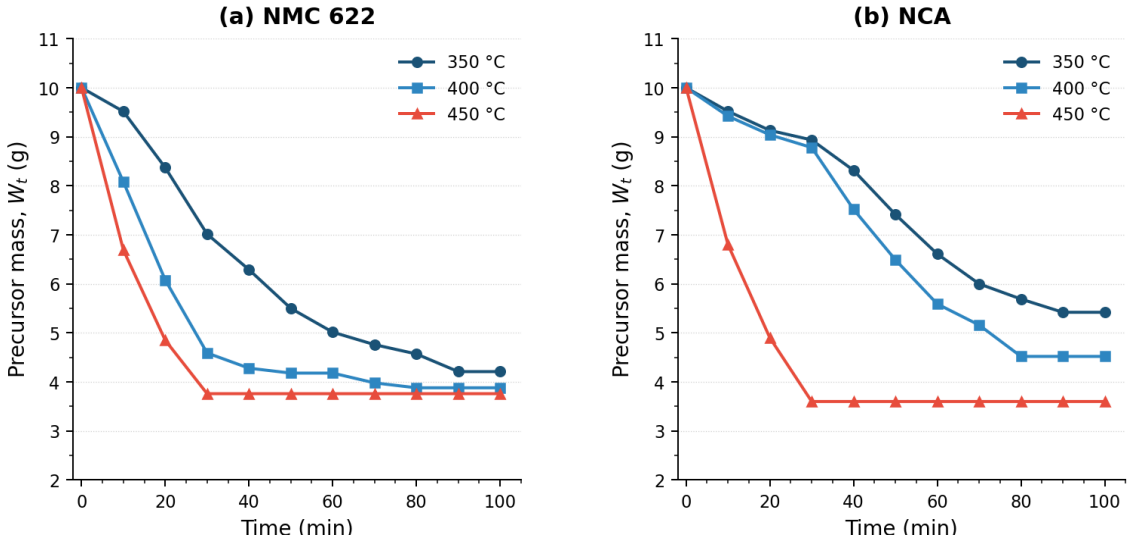

Figure 1. Isothermal mass-loss profiles of (a) NMC 622 and (b) NCA oxalate precursors at 350, 400, and 450 °C. Symbols: circles (350 °C), squares (400 °C), triangles (450 °C). Lines are guides to the eye.

The final stable masses (plateau values) were 3.8–4.2 g for both materials, corresponding to 38–42% mass retention — in reasonable agreement with the theoretical stoichiometric prediction of ~41% for complete conversion to a divalent mixed metal oxide (see Section 2.3). The slight variation reflects compositional differences (Al_2O_3 has a higher molecular weight per metal atom than NiO or CoO) and potential minor differences in initial hydration state between batches.

The NMC 622 profile shows a steeper initial gradient than NCA at equivalent temperatures, particularly at 350 °C, where NMC 622 loses approximately 5.8 g within 100 minutes compared to 4.6 g for NCA. This suggests that the NMC 622 oxalate is inherently more reactive towards thermal cleavage at lower temperatures. This trend is consistent with the lower activation energy determined for NMC 622.

3.3 Determination of Reaction Order

The integral kinetic method was applied to each dataset. For NMC 622, the first-order linearisation ($\ln(W_0/W_t)$ vs. t, Equation 2) produced substantially better fits (R^2 = 0.80–0.99) than the zero-order model at all temperatures. For NCA, the zero-order model ($W_0 - W_t$ vs. t, Equation 1) was consistently superior (R^2 = 0.86–0.99). The linearised plots and best-fit lines are shown in Figure 2, and the complete results are tabulated in Table 2.

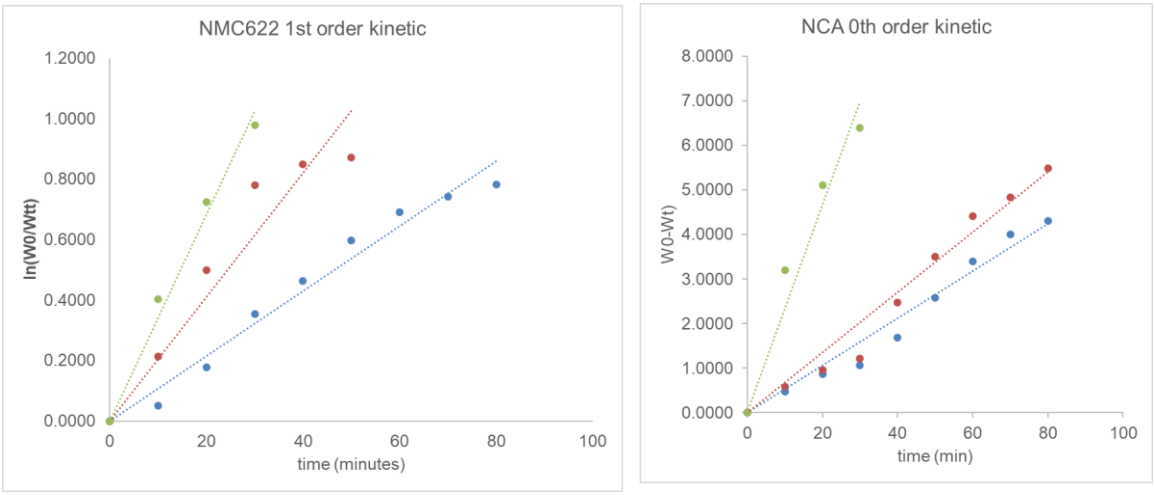

Figure 2. Integral kinetic linearisation plots: (a) first-order model for NMC 622, $\ln(W_0/W_t)$ vs. time; (b) zero-order model for NCA, (W_0-W_t) vs. time. Symbols: experimental data; dashed/dash-dot lines: linear regression (green 450, red 400, blue 350 °C)

Table 2. Best-fit kinetic rate constants and R^2 values from isothermal decomposition experiments. The two entries at 350 °C for NMC 622 represent independent replicate runs; their mean (k = 0.00465 min^{-1}) was used in the Arrhenius regression

T (°C)	Precursor	Best Order	k	R^2
350 (Run 1)	NMC 622	1st	0.0043 min^{-1}	0.9932
350 (Run 2)	NMC 622	1st	0.0050 min^{-1}	0.9882
400	NMC 622	1st	0.0065 min^{-1}	0.9367
450	NMC 622	1st	0.0104 min^{-1}	0.8022
350	NCA	0th	0.0674 g min^{-1}	0.9914
400	NCA	0th	0.0676 g min^{-1}	0.9891
450	NCA	0th	0.2329 g min^{-1}	0.9832

The first-order behaviour of NMC 622 is physically consistent with a reaction mechanism in which the rate-determining step involves the thermal cleavage of C–C or C–O bonds within the oxalate lattice at active sites distributed throughout the particle volume. As decomposition proceeds and the remaining oxalate mass diminishes, the number of active sites — and hence the reaction rate — decreases proportionally, giving first-order kinetics [9,10]. This mechanism is commonly observed for nickel, cobalt, and manganese oxalate decompositions in the literature [17,18].

The zero-order behaviour of NCA is more nuanced. Zero-order kinetics arise when the rate-limiting step is independent of the remaining reactant concentration — most commonly when mass or heat transport through a growing product layer controls the overall rate [19]. In the NCA

system, the decomposition of Al-containing oxalate generates Al_2O_3 as one of the product phases. Al_2O_3 is thermally stable (melting point ~2050 °C) and forms a relatively impermeable barrier compared to NiO, CoO, or MnO. The presence of this dense Al_2O_3 layer likely creates a diffusion barrier for outward migration of CO and CO_2 gases, thereby making gas-phase product removal the rate-limiting step and rendering the rate effectively constant (zero-order) with respect to remaining precursor mass [20]. A similar zero-order diffusion-limited mechanism has been proposed for alumina-containing composite systems [21].

The first-order kinetics for NMC 622 are consistent with the shrinking-core interface-reaction model [20], in which the rate decreases proportionally as the reactive solid surface diminishes during inward decomposition. For NCA, the zero-order behaviour is consistent with product-layer diffusion control within the same framework: the rate-limiting step is transport through a growing product layer, making the overall rate independent of the remaining precursor quantity [19]. Future structural studies — for example, XRD and SEM of partially calcined particles — could provide direct evidence for both proposed mechanisms.

3.4 Temperature Dependence of the Rate Constant

The rate constants extracted at each temperature are plotted on an Arrhenius diagram in Figure 3. The increase in k with temperature is monotonic for both materials, consistent with thermally activated kinetics. For NMC 622, k_1 increases from a mean value of 0.00465 min^{-1} at 350 °C (average of Groups 1 and 4) to 0.0104 min^{-1} at 450 °C, representing a 2.4-fold increase over 100 °C. For NCA, k_0 increases from 0.0674 g min^{-1} at 350 °C to 0.2329 g min^{-1} at 450 °C, a 3.5-fold increase — already suggesting a higher temperature sensitivity (larger E_a) for NCA relative to NMC 622.

It is noted that NCA data at 350 and 400 °C yield nearly identical k values (0.0674 and 0.0676 g min^{-1}), while a pronounced jump occurs at 450 °C. This non-uniformity in the temperature response may indicate a change in rate-limiting mechanism between 400 and 450 °C, or it may reflect experimental scatter exacerbated by the limited number of data points available at 450 °C (4 points compared to 9–11 at lower temperatures). The 450 °C data point is therefore treated with appropriate caution in the Arrhenius regression.

3.5 Arrhenius Parameters and Activation Energy

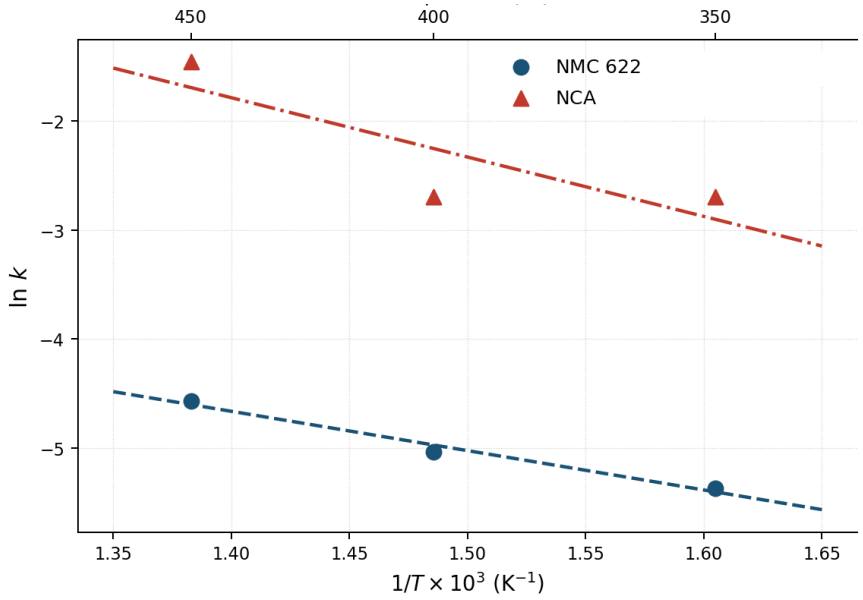

Figure 3. Arrhenius plots (ln k vs. 1/T) for NMC 622 (first-order, circles, navy) and NCA (zero-order, triangles, red). Regression lines are shown as dashed (NMC) and dash-dot (NCA). Error bars represent the range between replicate group values where available

Table 3. Arrhenius kinetic parameters for NMC 622 and NCA oxalate precursor decomposition

Precursor	Best-fit Order	Ea (kJ mol^{-1})	A	R^2 (Arrhenius)	Rate Law
NMC 622	1st	19.66	0.244 min^{-1}	0.907	$-dW/dt = k \cdot W$
NCA	0th	50.63	876.9 g min^{-1}	0.898	$-dW/dt = k$

The activation energy for NMC 622 first-order decomposition is E_a = 19.66 kJ mol^{-1} with a pre-exponential factor A = 0.244 min^{-1} and Arrhenius R^2 = 0.907. This value sits at the lower end of the range reported for individual binary transition metal oxalate decompositions (Ea ~ 15–80 kJ mol^{-1}) [10,11,22], consistent with the fact that NMC 622 is a mixed oxalate whose co-crystallised structure may have lower lattice energy compared to a pure binary compound due to strain and defect incorporation [23]. The relatively modest E_a value also implies that NMC 622 decomposition is not strongly sensitive to small temperature fluctuations within a furnace, which is advantageous for industrial-scale calcination where temperature uniformity across large powder beds is difficult to guarantee.

For NCA, E_a = 50.63 kJ mol^{-1} with A = 876.9 g min^{-1} and Arrhenius R^2 = 0.898. The higher activation energy confirms that NCA decomposition is kinetically more demanding and temperature-sensitive. The large pre-exponential factor A for NCA is an artefact of the zero-order rate law (A carries units of g min^{-1} and represents the product of the gas-solid collision frequency and the steric factor at the interface) and should not be directly compared to the A value of NMC 622 (units: min^{-1}). Literature values of E_a for diffusion-controlled solid decompositions typically fall in the range 40–80 kJ mol^{-1} [19,20], placing the NCA result squarely within the diffusion-controlled regime. The participation of

Al_2O_3 in constructing the product layer — with its significantly lower oxygen diffusivity relative to NiO [24] — is the most plausible physical explanation for the elevated E_a.

Comparative literature data for related cathode precursor systems are instructive. Qian et al. [25] found $E_a \sim 45$ kJ mol^{-1} for NCA hydroxide decomposition, somewhat lower than our NCA oxalate E_a, which may reflect the difference in precursor chemistry (oxalate vs. hydroxide) and the larger Al content promoting diffusion limitation in our oxalate system. A direct comparison is complicated by differences in heating mode (non-isothermal vs. isothermal), particle size distributions, and gas atmospheres, underscoring the need for system-specific kinetic characterization.

3.6 Implications for Calcination Process Optimisation

The kinetic parameters obtained here have direct, actionable implications for the design and optimisation of the calcination step in cathode material manufacturing. For NMC 622, the first-order rate law implies that the time required for a given fractional conversion $\alpha = (W_0 - W_t)/W_0$ scales as $t = -\ln(1 - \alpha)/k$. At 350 °C and using $k_1 = 0.00465$ min^{-1}, achieving 90% conversion requires approximately 495 minutes, while at 400 °C ($k = 0.0065$ min^{-1}) this reduces to 354 minutes. In practice, the observed plateau is reached in 80–100 minutes, suggesting that the effective conversion under experimental conditions exceeds the simple first-order model prediction once the rate decelerates markedly. This discrepancy may arise from particle size distributions and interparticle gas diffusion effects not captured by the lumped mass model.

For NCA, the zero-order rate law (constant mass-loss rate) gives $t = (W_0 - W_t)/k$, and the high activation energy means that a 50 °C temperature increase (e.g., 400 to 450 °C) reduces the required calcination time by a factor of approximately $\exp(E_a/R \times \Delta T/T^2) \approx 3.5$. This high temperature leverage is a double-edged sword: while it enables faster processing, it also means that local hot spots in an industrial furnace could generate significantly over-processed material (excess oxide phase growth, incipient sintering) relative to cooler zones, producing a heterogeneous product.

From a practical standpoint, a calcination temperature of 400 °C with a dwell time of 90 minutes in flowing air offers a viable processing window for both precursors. This condition ensures complete core decomposition while remaining safely below the thresholds (≥600 °C) where detrimental particle sintering and cation mixing occur. Furthermore, the low activation energy of NMC 622 (19.66 kJ mol^{-1}) implies low sensitivity to minor internal furnace temperature gradients. In contrast, the high E_a of NCA (50.63 kJ mol^{-1}) demands stringent spatial temperature uniformity within industrial reactors to prevent localized under- or over-calcination, highlighting a critical parameters for production scale-up. [3,6].

To contextualise the kinetic parameters obtained in this study, Table 4 presents a summary of activation energies reported for related metal oxalate and cathode precursor decompositions in the literature. The data show that binary transition metal oxalates typically decompose with E_a in the range 15–80 kJ mol^{-1} depending on the metal, atmosphere, and particle size. $NiC_2O_4 \cdot 2H_2O$ has been reported to decompose with $E_a \sim 18$–30 kJ mol^{-1} under non-isothermal conditions [10,11], closely bracketing the value of 19.66 kJ mol^{-1} determined here for NMC 622 — consistent with Ni being the dominant metal (60 mol%) in the NMC 622 composition. CoC_2O_4 decomposition

energies of 40–60 kJ mol^{-1} have been reported, attributable to the somewhat higher lattice energy of cobalt oxalate [22]. The intermediate E_a of the mixed NMC 622 system (19.66 kJ mol^{-1}) thus follows the expected trend of being dominated by the majority component (Ni), with minor contributions from Mn and Co.

For NCA, the value of 50.63 kJ mol^{-1} is substantially higher than would be expected from either NiC_2O_4 or CoC_2O_4 alone, supporting the proposed role of Al_2O_3 in elevating the effective barrier. Al_2O_3 formation from Al oxalate itself is reported to proceed with $E_a \sim$ 60–80 kJ mol^{-1} [21], and its presence as a minor but structurally significant product phase in NCA provides the mechanistic link between the high Al content and the elevated overall activation energy observed experimentally.

A potential limitation of the present kinetic analysis is the assumption of a single-step, single-order mechanism across the entire temperature and conversion range. In reality, the decomposition of a mixed metal oxalate hydrate is a multi-step process: (i) dehydration of crystal water (endothermic, typically 100–200 °C), (ii) decomposition of the anhydrous oxalate to oxide (endothermic, 250–450 °C), and (iii) possible reduction of intermediate oxide phases (e.g., NiO → Ni for reducing atmospheres) [9,17]. Under the conditions of this study (open-air calcination at 350–450 °C), steps (i) and (ii) likely overlap, particularly for the 10-minute interval data collection used here. The apparent rate constants therefore represent a lumped description of these overlapping processes rather than a true elementary rate constant. Differential scanning calorimetry (DSC) coupled with thermogravimetric analysis (TGA) would enable resolution of the individual steps, and future work should incorporate such measurements. Nevertheless, the lumped isothermal kinetic model is sufficient for the practical purpose of predicting dwell times and process temperatures for calcination, as demonstrated by its ability to reproduce the experimentally observed plateau times.

It should also be noted that the atmospheric composition (air vs. inert gas vs. controlled pO_2) affects the decomposition pathway and thermodynamics. In air, the formation of NiO, CoO, and MnO is thermodynamically stable at 350–450 °C, while in reducing atmospheres metallic Ni or Co could form [17]. The present study was conducted in stagnant air within a muffle furnace, with no forced gas flow. Controlled airflow would facilitate removal of CO and CO_2 product gases, potentially accelerating the rate by reducing local partial pressures and shifting the equilibrium of reaction (R5) to the right. This effect is expected to be more pronounced in the diffusion-limited NCA system, where CO_2 accumulation within the product layer could suppress the decomposition-driving force [20].

4. CONCLUSION

The isothermal decomposition kinetics of NMC 622 and NCA oxalate precursors were successfully quantified over a temperature range of 350–450 °C using the integral method. NMC 622 decomposition obeys a first-order rate law driven by mass availability, exhibiting a low activation energy (E_a = 19.66 kJ mol^{-1}) and rate constants ranging from 0.0043 to 0.0104 min^{-1}. Conversely, NCA decomposition follows a zero-order model (E_a = 50.63 kJ mol^{-1}) with rate constants of 0.0674–0.2329 $g.min^{-1}$, suggesting a transport-limited mechanism. Both materials achieve stable oxide plateaus within 90 minutes at 400 °C. The established Arrhenius parameters provide foundational engineering data required for thermal profile control and

reactor design during the scaling up of lithium-ion battery cathode precursor production.

ACKNOWLEDGMENT

The authors thank the University Center of Excellence for Electrical Energy Storage Technology (PUI-PT TPEL), Universitas Sebelas Maret, for the provision of laboratory facilities and reagents.

REFERENCES

[1] Liu, W., Oh, P., Liu, X., Lee, M.-J., Cho, W., Chae, S., Kim, Y., & Cho, J. (2015). Nickel-rich layered lithium transition-metal oxide for high-energy lithium-ion batteries. *Angew. Chem. Int. Ed.,* 54(15), 4440–4457. https://doi.org/10.1002/anie.201409262

[2] Manthiram, A., Knight, J. C., Myung, S.-T., Oh, S.-M., & Sun, Y.-K. (2016). Nickel-rich and lithium-rich layered oxide cathodes: progress and perspectives. Adv. *Energy Mater*., 6(1), 1501010. https://doi.org/10.1002/aenm.201501010

[3] Li, W., Erickson, E. M., & Manthiram, A. (2020). High-nickel layered oxide cathodes for lithium-based automotive batteries. *Nat. Energy*, 5(1), 26–34. https://doi.org/10.1038/s41560-019-0513-0

[4] Donkova, B., Vasileva, P., Nihtianova, D., Velichkova, N., Stefanov, P., & Mehandjiev, D. (2011). Synthesis, structural characterization, and catalytic application of CuxZn1−xO solid solutions obtained from oxalate precursors. *J. Mater. Sci.,* 46(21), 7134–7143. https://doi.org/10.1007/s10853-011-5650-y

AUTHOR CONTRIBUTION

The research experiment and writing article was carried out by Khikmah Nur Rikhy Stulasti, Aleida Dwi Rahmawati, Latriva Nur Aini, Anis Fitriani, and Naurani Zamruda. Supervision and review article by Himmah Sekar Eka Ayu Gustiana. Conceptualization and wrote final article by Cornelius Satria Yudha. The final report was committed by all contributors.

[5] Courty, P., Ajot, H., Marcilly, C., & Delmon, B. (1973). Oxydes mixtes ou en solution solide sous forme très divisée obtenus par décomposition thermique de précurseurs amorphes. *Powder Technol*., 7(1), 21–38. https://doi.org/10.1016/0032-5910(73)80004-9

[6] Ryu, H.-H., Park, K.-J., Yoon, C. S., & Sun, Y.-K. (2018). Capacity fading of Ni-rich Li[NixCoyMn1−x−y]O2 (0.6 ≤ x ≤ 0.95) cathodes for high-energy-density lithium-ion batteries: bulk or surface degradation? *Chem. Mater*., 30(3), 1155–1163. https://doi.org/10.1021/acs.chemmater.7b05269

[7] Sun, H., & Zhao, K. (2017). Electronic structure and comparative properties of LiNixMnyCozO2 cathode materials. *J. Phys. Chem. C*, 121(11), 6002–6010. https://doi.org/10.1021/acs.jpcc.7b00810

[8] Kim, U.-H., Ryu, H.-H., Kim, J.-H., Mücke, R., Kaghazchi, P., Yoon, C. S., & Sun, Y.-K. (2019). Microstructure-controlled Ni-rich cathode material by microscale compositional partition for next-generation electric vehicles. *Adv. Energy Mater*., 9(15), 1803902. https://doi.org/10.1002/aenm.201803902

[9] Brown, M. E., Dollimore, D., & Galwey, A. K. (1980). Reactions in the Solid State. *Comprehensive Chemical Kinetics,* Vol. 22. Elsevier, Amsterdam. ISBN: 978-0-444-41807-3

[10] Dollimore, D., Griffiths, D. L., & Nicholson, D. (1963). The thermal decomposition of various oxalates in air and in nitrogen. *J. Chem. Soc*., 2617–2623. https://doi.org/10.1039/JR9630002617

[11] Dollimore, D. (1987). The thermal decomposition of oxalates: a review. *Thermochim. Acta,* 117, 331–363. https://doi.org/10.1016/0040-6031(87)88023-1

[12] Baes, C. F., & Mesmer, R. E. (1976). The Hydrolysis of Cations. *Wiley-Interscience,* New York. ISBN: 978-0-471-03985-7

[13] Yue, P., Wang, Z., Li, X., Xiong, X., Wang, J., Wu, X., & Guo, H. (2013). The enhanced electrochemical performance of Li[Ni0.6Co0.2Mn0.2]O2 cathode material by a low temperature Co-precipitation method. *Electrochim. Acta,* 95, 112–118. https://doi.org/10.1016/j.electacta.2013.02.029

[14] Maciejewski, M., Ingier-Stocka, E., Emmerich, W. D., & Baiker, A. (2000). Monitoring of the gas phase composition: a prerequisite for unravelling the mechanism of decomposition of solids. Thermal decomposition of cobalt oxalate dihydrate. *J. Therm. Anal. Calorim*., 60, 735–758. https://doi.org/10.1023/A:1010135003141

[15] Martell, A. E., & Smith, R. M. (2004). NIST Standard Reference Database 46: Critically Selected Stability Constants of Metal Complexes, Version 8.0. *National Institute of Standards and Technology*, Gaithersburg, MD. https://www.nist.gov/srd/nist46

[16] Chang, R., & Kim, J. H. (2014). Infrared spectroscopic analysis and co-precipitation synthesis of mixed transition metal oxalates for lithium-ion battery applications. *Journal of Power Sources*, 251, 142–149. https://doi.org/10.1016/j.jpowsour.2013.11.022

[17] Galwey, A. K., & Brown, M. E. (1999). Thermal Decomposition of Ionic Solids: Chemical Properties and Reactivities of Ionic Crystalline Phases. *Studies in Physical and Theoretical Chemistry*, Vol. 86. Elsevier, Amsterdam. ISBN: 978-0-444-82437-5

[18] Abd El-Salaam, K. M., & Hassan, E. A. (1982). Kinetics of the thermal decomposition of nickel oxalate. *Surf. Technol*., 16(3), 179–188. https://doi.org/10.1016/0376-4583(82)90023-7

[19] Khawam, A., & Flanagan, D. R. (2006). Solid-state kinetic models: basics and mathematical fundamentals. *J. Phys. Chem. B,* 110(35), 17315–17328. https://doi.org/10.1021/jp062746a

[20] Levenspiel, O. (1999). Chemical Reaction Engineering (3rd ed.). *John Wiley & Sons,* New York, pp. 376–392. ISBN: 978-0-471-25424-9

[21] Wefers, K., & Misra, C. (1987). Oxides and Hydroxides of Aluminum. *Alcoa Technical Paper* No. 19, Alcoa Laboratories, pp. 45–52

[22] Muraleedharan, K., Kannan, M. P., & Gangadevi, T. (1994). The thermal decomposition of cobalt oxalate dihydrate in flowing atmospheres of different gases. *Thermochim. Acta,* 232(2), 187–197.

https://doi.org/10.1016/0040-6031(94)80059-6

[23] Shannon, R. D. (1976). Revised effective ionic radii and systematic studies of interatomic distances in halides and chalcogenides. *Acta Crystallogr.* Sect. A, 32(5), 751–767. https://doi.org/10.1107/S0567739476001551

[24] Atkinson, A. (1985). Transport processes during the growth of oxide films at elevated temperature. *Rev. Mod. Phys.,* 57(2), 437–470. https://doi.org/10.1103/RevModPhys.57.437

[25] Qian, G., Li, T., Zhao, P., & Liang, J. (2020). Thermal stability and decomposition kinetics of NCA cathode hydroxide precursors. *J. Therm. Anal. Calorim.*, 139(2), 1313–1321. https://doi.org/10.1007/s10973-019-08547-0